

Effect of soil-structure interaction on seismic damage of mid-rise reinforced concrete structures retrofitted by FRP composites

Vui Van Cao*

Faculty of Civil Engineering, Ho Chi Minh city University of Technology (HCMUT)-Vietnam National University,
268 Ly Thuong Kiet Street, District 10, Ho Chi Minh city, Vietnam

(Received May 4, 2018, Revised June 14, 2018, Accepted June 27, 2018)

Abstract. The current study explores the soil-structure interaction (SSI) effect on the potential seismic damage of mid-rise non-seismically designed reinforced concrete frames retrofitted by Fibre Reinforced Polymer (FRP). An 8-storey reinforced concrete frame poorly-confined due to transverse reinforcement deficiency is selected and then retrofitted by FRP wraps to provide external confinement. The poorly-confined and FRP retrofitted frames with/without SSI are modelled using hysteretic nonlinear elements. Inelastic time history and damage analyses are performed for these frames subjected to different seismic intensities. The results show that the FRP confinement significantly reduces one or two damage levels for the poorly-confined frame. More importantly, the SSI effect is found to increase the potential seismic damage of the retrofitted frame, reducing the effectiveness of FRP retrofitting. This finding, which is contrary to the conventionally beneficial concept of SSI governing for decades in structural and earthquake engineering, is worth taking into account in designing and evaluating retrofitted structures.

Keywords: soil-structure interaction; damage; reinforced concrete frame; earthquake; FRP

1. Introduction

Over the last few decades, the issue of soil-structure interaction (SSI) has been increasingly investigated by research community. Researchers seem to be unanimous that the SSI results in increasing the effective damping and decreasing the stiffness of SSI systems. Consequently, the response of a structure with SSI has been proven to be significantly different from that of the same structure with fixed bases (Chopra and Gutierrez 1974). On the contrary, researchers have been inconsistent in answering the question: "Is the SSI effect beneficial or detrimental?". Particularly, majority of researchers came up with the conclusion that the interaction results in either beneficial or detrimental effects on structures (Avilés and Pérez-Rocha 2003, Jarernprasert *et al.* 2013, Jennings and Bielak 1973, Mason *et al.* 2013, Mylonakis and Gazetas 2000, Nakhaei and Ali Ghannad 2008, Sáez *et al.* 2011, Veletsos and Meek 1974) while others concluded that the interaction is detrimental (Dutta *et al.* 2004, Ghandil and Behnamfar 2017, Halabia and Zafaran 2014, Halabian and Emami 2014, Hassani *et al.* 2018, Papagiannopoulos 2017).

In seismic design codes (ASCE 2010, FEMA750 2009), the effect of SSI is ignored or considered by reducing the design base shear of fixed base structures. The idea behind this regulation is that the increase of the fundamental period due to SSI effect will be beneficial to the response of structures. The SSI effect in these codes has been based mainly on elastic single degree of freedom (SDOF) systems

conducted by Bielak (1971), Jennings and Bielak (1973), Veletsos and Meek (1974). These elastic SDOF systems may result in two major limitations: 1) only the first mode of structures is taken into account; ignoring higher modes which, however, play important roles in case of multistorey buildings, especially mid-rise and high-rise buildings; 2) inelasticity and damage of structures occurring during earthquake excitations cannot be captured by these elastic SDOF systems.

Comparing to requirements in modern codes, many existing buildings around the world have been identified to be deficient. One of universal deficiencies is of transverse reinforcement. Seismic design of transverse reinforcement has been considerably changed as the concept of ductile structures was implemented. Deficiency of transverse reinforcement leads to none or low confinement for concrete, resulting in low ductility; consequently, structures suffer severe damage or collapse as evident in the past earthquakes such as Northridge in 1994, Kobe in 1995, Chi-Chi in 1999, Bam in 2003, Christchurch in 2011 and most recently Hualien in 2018. After these events, deficient buildings in other seismic regions have been in middle of the two decisions: 1) strengthening to meet the seismic demand or 2) demolishing and rebuilding. The second solution seems to be costly and non-preferable. Fortunately, Fibre Reinforced Polymer (FRP) with its distinct properties such as high strength, lightweight and ease of application has made strengthening become a solution of choice.

Research on strengthening of deficient reinforced concrete (RC) structures using FRP has been extensively conducted by many researchers. FRP strengthening significantly improves the mechanical properties of concrete (Lam and Teng 2003a, Pellegrino and Modena 2010, Samaan *et al.* 1998, Smith *et al.* 2010, Wei and Wu

*Corresponding author, Lecturer
E-mail: cvvui@hcmut.edu.vn

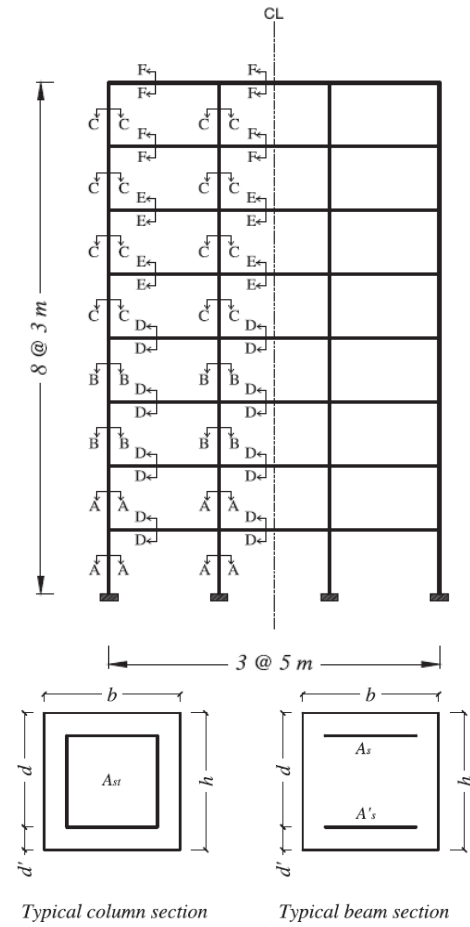


Fig. 1 Poorly-confined 8-storey frame and its typical column and beam sections (Eslami and Ronagh 2013, Ronagh and Eslami 2013)

2012), results in better performance of RC members (Adibi *et al.* 2017, Harajli and Rteil 2004, Hawileh *et al.* 2015, Kuntal *et al.* 2017, Rahai and Akbarpour 2014a, 2014b, Reda *et al.* 2016, Sheikh and Yau 2002) and substantially increases the seismic capacity of RC frames (Balsamo *et al.* 2005, Eslami and Ronagh 2013, Garcia *et al.* 2010, Güneyisi and Azez 2016, Kakaletsis 2016, Ludovico *et al.* 2008, Ludovico *et al.* 2008, Mortezaei *et al.* 2010). FRP strengthening also reduces the structural damage of RC frames subjected to earthquake excitations (Cao and Ronagh 2014).

However, the above mentioned studies (Balsamo *et al.* 2005, Cao and Ronagh 2014, Eslami and Ronagh 2013, Garcia *et al.* 2010, Güneyisi and Azez 2016, Kakaletsis

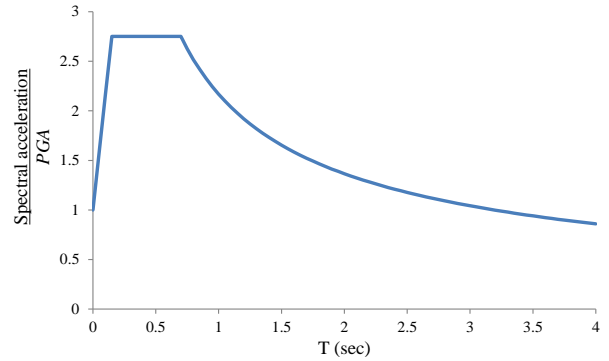


Fig. 2 Spectral acceleration/PGA

2016, Ludovico *et al.* 2008, Ludovico *et al.* 2008, Mortezaei *et al.* 2010) were conducted for RC frames supported on fixed bases which are conventionally used in structural analysis. None of them included the effect of SSI which is an inevitable phenomenon occurring during earthquakes. The current study is aiming at the effect of SSI on the potential damage of mid-rise RC frames retrofitted by FRP subjected to different seismic intensities. For this aim, an 8-storey RC frame poorly-confined due to deficiency of transverse reinforcement is chosen to represent mid-rise structures. The frame is then retrofitted using FRP wraps to provide external confinement. The poorly-confined and retrofitted frames supported on fixed bases (without SSI) and flexible bases (with SSI) are modelled in SAP2000 (Computers and Structures Inc 2017) using hysteretic nonlinear LINK elements. Inelastic time history analyses are performed for these frames subjected to different seismic intensities. The data obtained from inelastic time history analyses are then used for computing damage indices. The damage indices and damage distribution in the FRP retrofitted frame with and without SSI are compared with each other and with those in the original frame. Conclusions are made based on the comparisons.

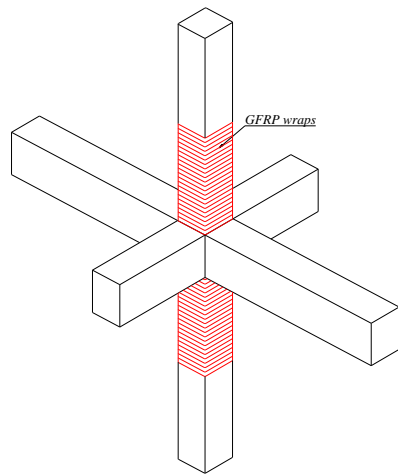
2. Descriptions of poorly-confined and FRP-confined retrofitted 8-storey frames

2.1 Poorly-confined 8-storey frame

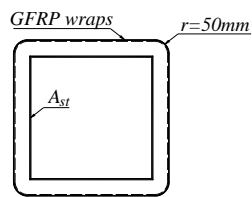
The poorly-confined 8-storey RC frame in the Refs. (Eslami and Ronagh 2013, Ronagh and Eslami 2013) is selected to represent mid-rise structures. Fig. 1 shows the frame and its typical cross sections while Table 1 shows the

Table 1 Reinforcement details (Eslami and Ronagh 2013)

Section	<i>b</i> (mm)	<i>h</i> (mm)	<i>d</i> (mm)	<i>d'</i> (mm)	<i>A_{st}</i>	<i>A_s</i>	<i>A'_s</i>	Shear steel spacing (mm)
A-A	600	600	540	60	16Φ25	-	-	450
B-B	600	600	540	60	16Φ18	-	-	450
C-C	500	500	440	60	16Φ16	-	-	450
D-D	500	500	440	60	-	6Φ25	4Φ25	140
E-E	500	500	440	60	-	6Φ22	4Φ22	175
F-F	500	500	440	60	-	6Φ18	3Φ18	250

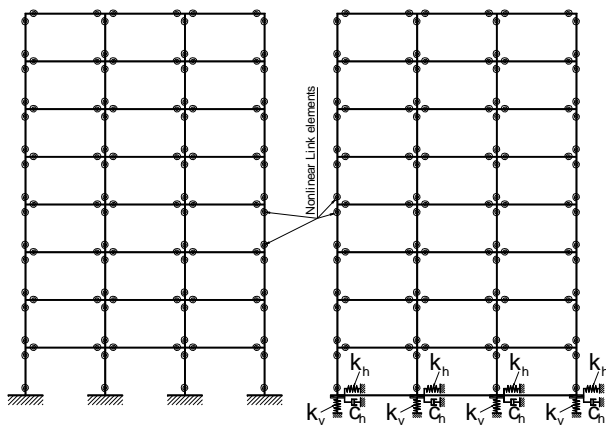


(a) General view



(b) Cross section

Fig. 3 Design of GFRP wraps



(a) Fixed bases

(b) With SSI

Fig. 4 Models of 8-storey frames

details of longitudinal reinforcement and poorly-confined transverse steel. The compressive strength of concrete was 25 MPa and yield stress of steel was $f_y=420$ MPa. Steel $\Phi 10$ mm was used for transverse reinforcement.

The design gravity load includes 30 kN/m Dead Load, 10 kN/m Live Load and the self-weight of the structure. The lateral seismic load was designed based on UBC code (1994). The frame was assumed to locate in a region of high seismic hazard with peak ground acceleration (PGA) of 0.3g and soil class D regulated in FEMA 356 (ASCE 2000). Fig. 2 shows the design response spectrum divided by PGA.

2.2 FRP-confined retrofitted 8-storey frame

Due to the deficiency of transverse reinforcement

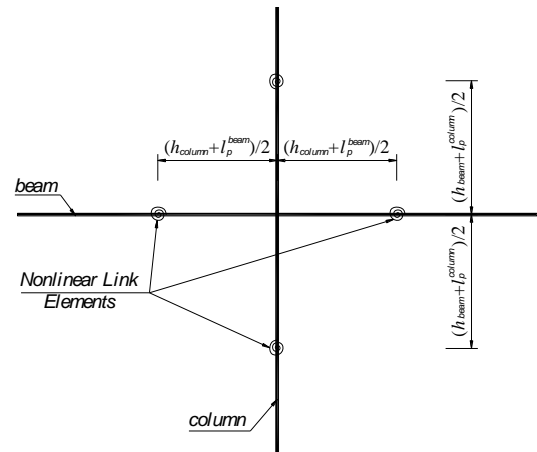


Fig. 5 Locations of nonlinear LINK elements

leading to none or low internal confinement, providing external confinement will be an appropriate retrofitting solution. Thus, external confinement by FRP is added. Comparing to CFRP, GFRP was identified as a suitable choice for confinement retrofitting (Cao and Ronagh 2014, Eslami and Ronagh 2013) and is used in this study. The tensile strength, tensile modulus and thickness of GFRP unidirectional fibre sheets provided by the manufacturers are 3241 MPa, 72379 MPa and 0.589 mm, respectively (Luca *et al.* 2011). The retrofitting design is shown in Fig. 3, in which the columns are wrapped by two GFRP layers. The length of GFRP wrapped column is designed to be twice of the plastic hinge length. Column corners should be rounded in order to improve the effectiveness of GFRP wrap (Wang and Wu 2008). Thus, 50 mm rounding at column corners is applied as shown in Fig. 3(b).

It is worth mentioning that the GFRP wraps do not affect the locations of plastic hinges as reported in the study on FRP retrofitted columns (Sheikh and Yau 2002). In addition, GFRP is not applied to beams. Thus, the plastic hinge locations in beams and columns of the retrofitted and original frames are similar.

3. Modelling

Fig. 4(a) shows the model of 8-storey frame with fixed bases while Fig. 4(b) illustrates the model of the frame with SSI. The modelling comprises two main parts: modelling of RC structures presented in Section 3.1 and modelling of SSI described in Section 3.2.

3.1 Modelling of RC frames

The modelling technique is briefly described herein and its details can be found in Ref. (Cao and Ronagh 2014). The frame is modelled using two element types: elastic elements and inelastic elements. Inelastic elements are the hysteretic nonlinear LINK elements. Locations of these elements are shown in Fig. 5, in which, l_p^{beam} and l_p^{column} are the plastic hinge length of beams and columns, respectively. The hysteretic nonlinear LINK element employs the moment-

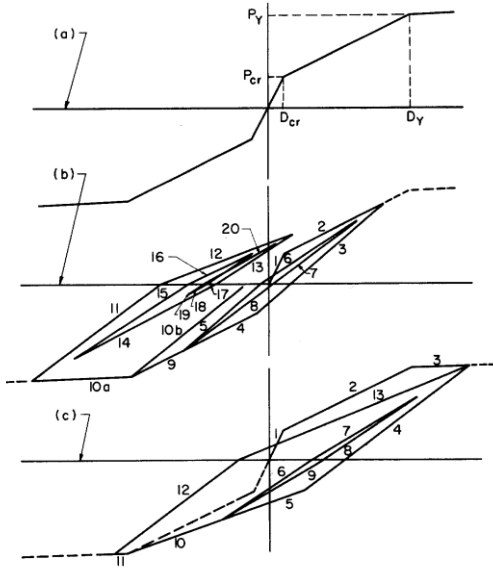


Fig. 6 Load-displacement relationship (Takeda *et al.* 1970)

rotation property of the plastic hinge and behaves in accordance with a hysteretic model. Amongst hysteretic models available in literature, Takeda model (Takeda *et al.* 1970) includes the crack of concrete which is considered a starting point of damage as shown in Fig. 6(a), in which (D_{cr}, P_{cr}) and (D_y, P_y) are the coordinates of cracking and yielding points, respectively; thus, it is selected to use in this paper. Fig. 6(b) and 6(c) briefly show seven rules developed by Takeda *et al.* (1970). The details of these seven rules can be found in Ref (Takeda *et al.* 1970).

Moment-rotation curves are obtained from moment-curvature curves and the plastic hinge length. Fibre model is used for moment-curvature analyses performing for beams and columns at the plastic hinge zones while the plastic hinge length $l_p=h$ proposed by Sheikh and Houry (1993) is adopted. The average axial forces in columns and beams during an earthquake are used in these analyses. The ultimate curvature is corresponding to the state that the longitudinal steel or concrete reaches its ultimate strain whichever comes first. The ultimate strain of longitudinal steel ε_{sm} is shown in Eq. (1) and that of concrete ε_{cm} is shown in Eq. (2) (Paulay and Priestley 1992).

$$\varepsilon_{sm} = 0.6\varepsilon_{su} \quad (1)$$

$$\varepsilon_{cm} = 0.004 + 1.4 \frac{\rho_s f_{yh} \varepsilon_{sub}}{f_{cc}} \quad (2)$$

Among different available models of stress-strain relationship for concrete confined by rectangular transverse reinforcement, the Park *et al.* (1982) model, which is a modification of Kent and Park (1971) model, is used in this paper because it includes enhancements of strength, strain corresponding to peak stress and the descending branch of confined concrete. The Park *et al.* (1982) model is described by Eqs. (3)-(4), followed by Eqs. (5)-(8).

$$f_c = f_c^* \left[\frac{2\varepsilon_c}{\varepsilon_o} - \left(\frac{\varepsilon_c}{\varepsilon_o} \right)^2 \right] \quad \text{if } \varepsilon_c \leq \varepsilon_o \quad (3)$$

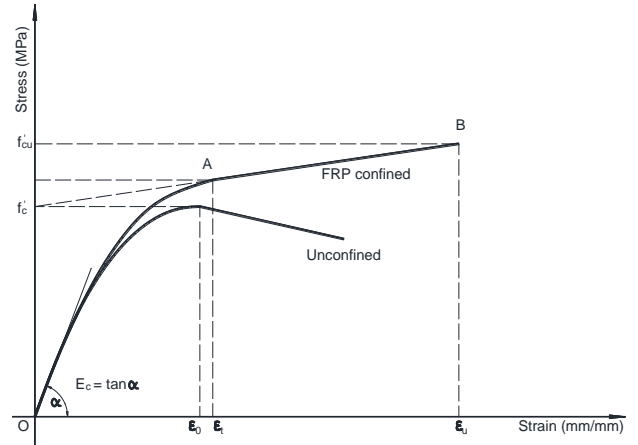


Fig. 7 Model of FRP confined concrete (Lam and Teng 2003a, 2003b)

$$f_c = f_c^* [1 - Z(\varepsilon_c - \varepsilon_o)] \geq 0.2f_c^* \quad \text{if } \varepsilon_c \geq \varepsilon_o \quad (4)$$

where,

$$f_c^* = Kf_c' \quad (5)$$

$$\varepsilon_o = 0.002K \quad (6)$$

$$Z = \frac{0.5}{\frac{3 + 0.29f_c'}{145f_c' - 1000} + \frac{3}{4}\rho_s \sqrt{\frac{b''}{s_h}} - 0.002K} \quad (7)$$

$$K = 1 + \frac{\rho_s f_{yh}}{f_c'} \quad (8)$$

in which, f_c is the concrete stress and ε_c is the concrete strain; ρ_s is the ratio of the volume of rectangular steel hoops to the volume of concrete core measured to the outside of the peripheral hoop; f_c' is the maximum stress in MPa; b'' is the width of the concrete core measured to outside of the peripheral hoop; s_h is the spacing of stirrups.

Past studies (Harajli *et al.* 2006, Lam and Teng 2003a, 2003b, Wei and Wu 2012, 2007, 2007) proved that the mechanical properties of concrete are significantly increased if confined by FRP. For RC members wrapped by FRP, the concrete core surrounded by stirrups is confined both externally by FRP and internally by transverse reinforcement while the concrete cover is confined only by FRP. To simplify, the poor confinement of deficient transverse reinforcement is neglected when the FRP confinement becomes effective. The stress-strain model of concrete confined by FRP proposed by Lam and Teng (2003a, 2003b) illustrated in Fig. 7 is adopted in this study because it is appropriate for rectangular columns (Rocca *et al.* 2009). This model is expressed by Eqs. (9)-(10), followed by Eqs. (11)-(20).

Branch OA ($0 \leq \varepsilon_c \leq \varepsilon_t$):

$$f_c = E_c \varepsilon_c - \frac{(E_c - E_2)^2}{4f_c'} \varepsilon_c^2 \quad (9)$$

Branch AB ($\varepsilon_t \leq \varepsilon_c \leq \varepsilon_u$):

$$f_c = f'_c + E_2 \varepsilon_c \quad (10)$$

in which

$$\varepsilon_c = \frac{2f'_c}{E_c - E_2} \quad (11)$$

$$E_2 = \frac{f'_{cu} - f'_c}{\varepsilon_u} \quad (12)$$

where, E_c is the elastic modulus of concrete, $E_c = 4700\sqrt{f'_c}$ (ACI 2008);

f'_{cu} and ε_u are the stress and strain at ultimate.

$$f'_{cu} = f'_c \left[1 + 3.3k_{s1} \frac{f_{la}}{f'_c} \right] \quad \text{if } \frac{f_{la}}{f'_c} \geq 0.07 \quad (13)$$

$$f'_{cu} = f'_c \quad \text{if } \frac{f_{la}}{f'_c} < 0.07 \quad (14)$$

$$\varepsilon_u = \varepsilon_o \left[1.75 + 12k_{s2} \frac{f_{la}}{f'_c} \left(\frac{\varepsilon_{h,rup}}{\varepsilon_o} \right)^{0.45} \right] \quad (15)$$

$$f_{la} = \frac{E_f t_f}{R} \varepsilon_{h,rup} = \frac{2E_f t_f}{D} \varepsilon_{h,rup} \quad (16)$$

where, t_f and E_f are the thickness and modulus of the FRP wrap; D is the equivalent diameter as shown in Eq. (17); k_{s1} and k_{s2} are shape factors; b and h are the width and the depth of the cross section; r is the radius of the corner; ρ_s is the ratio of longitudinal steel reinforcement.

$$D = \sqrt{h^2 + b^2} \quad (17)$$

$$k_{s1} = \left(\frac{b}{h} \right)^2 \frac{A_e}{A_c} \quad (18)$$

$$k_{s2} = \left(\frac{h}{b} \right)^{0.5} \frac{A_e}{A_c} \quad (19)$$

$$\frac{A_e}{A_c} = \frac{1 - \left((b/h)(h-2r)^2 + (h/b)(b-2r)^2 \right) / (3A_g) - \rho_s}{1 - \rho_s} \quad (20)$$

$\varepsilon_{h,rup} = k_c \varepsilon_{frp}$ is the rupture strain of GFRP, in which k_c is ‘‘FRP strain efficiency factor’’, This factor has been recommended as 0.624 by Lam and Teng (2003a), 0.68 by Realfonzo and Napoli (2013) and 0.66 by Baji *et al.* (2016). Comparing the first value with the second and the third ones, the differences are 8.2% and 5.5%, respectively. Also, it is worth mentioning that these strain efficiency factors are of circular specimens under monotonic axial loading. The strain reduction factor in case of rectangular section and cyclic loading could be smaller than the above mentioned factors due to higher stress at corners and further investigation on this issue should be encouraged. Thus, the smallest of the three above factors, 0.624, which is close to

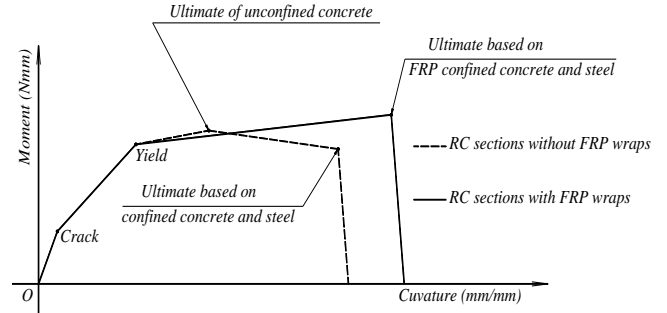


Fig. 8 Moment-curvature curves of a section with and without FRP wraps

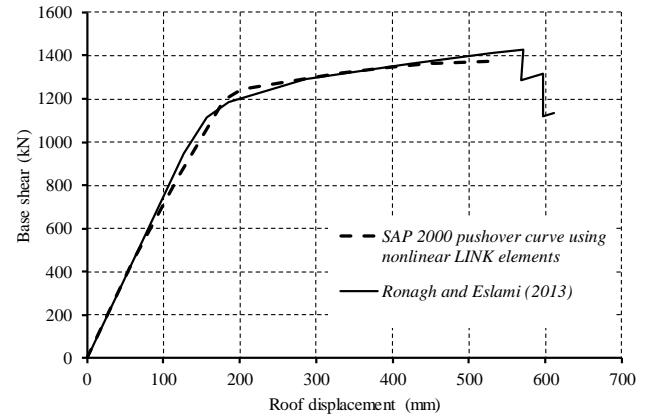


Fig. 9 Pushover curves

the value 0.62 recently recommended by Baji (2017), is used in the current paper.

Fig. 8 illustrates typical moment-curvature curves for a section with and without FRP wrap. Cracking, yielding and ultimate points are included in these curves. The curves up to yield are similar; however, difference can be seen after the yield point. These similarity and difference can be explained by the FRP confinement effect as observed in Lam and Teng (2003a, 2003b) model shown in Fig. 8. The ultimates are based on the ultimate of the confined concrete and that of the steel whichever occurs first. The moment-curvature of a section without FRP includes the ultimate of unconfined concrete. The post-ultimate moment is assumed to drop to 0.

Under full Dead Load and 25% Live Load, the fundamental period $T=1.24s$ is determined, showing a good agreement with the period 1.28s modelled by Ronagh and Eslami (2013). Base shear force is computed and distributed vertically based on building code (ICBO 1994). Pushover analysis is then performed for the frame. The obtained pushover curve is comparable to the curve analysed by Ronagh and Eslami (2013) and an overall approximation can be observed in Fig. 9.

3.2 Modelling of SSI

In order to determine the SSI parameters, a layout of pile footing system as shown in Fig. 10 is assumed. The plan of footing system is illustrated in Fig. 10(a) while the side view is shown in Fig. 10(b). Each first storey column is

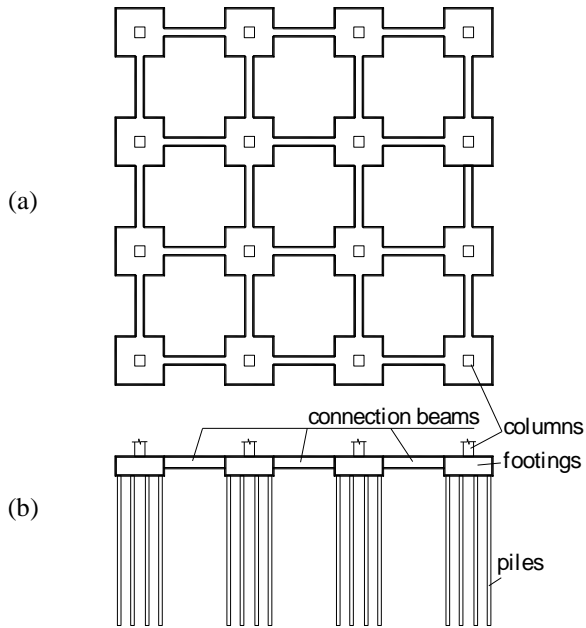


Fig. 10 Footing system: (a) plan; (b) side view

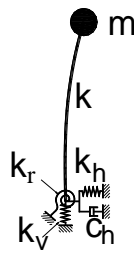


Fig. 11 SDOF system with SSI

on its footing. Footings are connected by beams. The SSI mainly depends on top soil layer which surrounds footing system. The top layer surrounding footings is assumed to be soft soil which has shear wave velocity $V_s=90$ m/s.

A structure supported on a stand-alone single footing can be modelled as SDOF system shown in Fig. 11. The SSI properties include a translational spring with stiffness k_h , a damping c_h , a rotational spring with stiffness k_r and a vertical spring with stiffness k_v .

The rotational spring significantly contributes to the lateral displacement of the SDOF system. However, in a frame structure supported on the footing system shown in Fig. 10, the rotation of an individual footing is prevented by the connection beams and other footings. Thus, this rotation is neglected in the SSI frame model.

The horizontal SSI is assumed to mainly occur on the sides of footings and connection beams. This interaction is important during earthquake excitation because it is close to the frame structure and importantly contributes to horizontal displacement of the frame. On the contrary, the horizontal interaction between soil and piles may play a minor role as its location is in lower soil layers and the piles can be bent. The vertical stiffness of the pile footings is assumed to be large because pile ends are normally located in deep stiff soil layers. Thus, the vertical displacement of footing system is ignored. The relative translational

stiffness k_h and the damping c_h are calculated using Eqs. (21)-(22) (Jareernprasert 2005, Jareernprasert *et al.* 2013), respectively. The ratio of fundamental period of a system with SSI to that of a system with fixed bases can be approximately by Eq. (23) (Bielak 1971)

$$\frac{k}{k_h} = \frac{2860}{V_s^2} \left(\frac{H}{B}\right)^{-1} \left(1 + 0.234 \frac{H}{B}\right)^{-1} \quad (21)$$

$$C_h = \frac{\beta_o \frac{kT}{\pi} \lambda^3}{\left(\frac{k}{k_h}\right)^2} + \frac{k_h T}{\pi} \lambda D \quad (22)$$

$$\lambda = \frac{T'}{T} = \sqrt{1 + \frac{k}{k_h}} = \sqrt{1 + \frac{2860}{V_s^2} \left(\frac{H}{B}\right)^{-1} \left(1 + 0.234 \frac{H}{B}\right)^{-1}} \quad (23)$$

in which, V_s is the shear wave velocity (m/s) of the elastic half space; H is the height of structure; B is the dimension of foundation; k is the translational stiffness of fixed-base frame; T is the fundamental period of fixed-base frame; T' is the fundamental period of the frame with SSI; $D=0.05$ is the linear hysteretic damping ratio of soil.

Assuming the damping ratio of the fixed-based structure is 5%. The mass of footings is approximately 104 ton which is assumed to be 20% the mass of superstructure (Jareernprasert *et al.* 2013). The soil damping ratio $\beta_o=0.1$, which was used in by Shakib and Fuladgar (2004) and Zamani and El Shamy (2014), is adopted in the current study and the soil damping is determined as 29156.8 kN/(m/s). The translational stiffness k of fixed-base frame is determined from the pushover curves in Fig. 9. Using Eq. (21), the lateral stiffness of soil surrounding footings k_h is computed as 46534.6 kN/m. The parameter

$$\lambda = \frac{T'}{T} = \sqrt{1 + \frac{k}{k_h}} = 1.08 \quad \text{and thus, the computed}$$

fundamental period $T' = \lambda T = 1.08 \times 1.24 = 1.34$ s while the fundamental period of the structure with SSI obtained from SAP2000 model is 1.38157 s, showing a good agreement.

4. Inelastic time history and damage analyses

The load using for inelastic time history analyses includes 100% Dead Load and 25% Live Load as recommended in many seismic codes. The frames are subjected to three sets of seismic intensities with PGA of 0.3g, 0.45g and 0.6g. Each set includes 14 records which are fault-normal and fault-parallel components at 7 stations. These records are selected from PEER database (PEER 2011) and then scaled to match the target response spectrum established for the above three intensities. The match is in the range of period from $0.2T$ to $1.5T$, where $T=1.24$ s is the first period of the structure. The selected records, scaling factors and Next Generation Attenuation number (NGA#) are presented in Table 2.

Inelastic time history analyses are performed for three cases: 1) the poorly-confined frame with fixed bases; 2) the

Table 2 Selected records and scaling factors for three seismic intensities

No.	NGA#	Scale Factor for intensity of			Event	Year	Station	Magnitude
		0.3g	0.45g	0.6g				
1	1497	2.8719	4.3074	5.7432	Chi-Chi, Taiwan	1999	TCU057	7.62
2	1215	5.5179	8.2761	11.035	Chi-Chi, Taiwan	1999	CHY058	7.62
3	1488	3.1241	4.6857	6.2476	Chi-Chi, Taiwan	1999	TCU048	7.62
4	3441	32.4018	48.5983	64.798	Chi-Chi, Taiwan-06	1999	TCU007	6.3
5	2822	31.6713	47.5026	63.337	Chi-Chi, Taiwan-04	1999	KAU055	6.2
6	3537	15.0175	22.5242	30.032	Chi-Chi, Taiwan-06	1999	TTN032	6.3
7	1243	4.9909	7.4857	9.9809	Chi-Chi, Taiwan	1999	CHY100	7.62

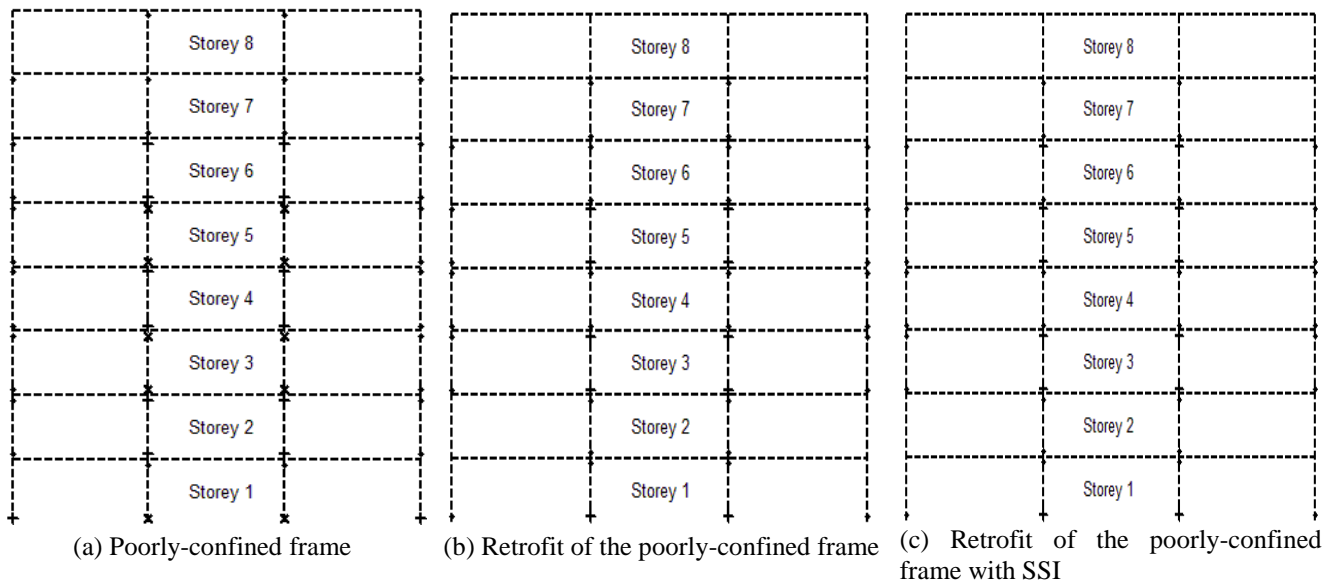


Fig. 12 Damage modes of 8-storey frames under seismic intensity 0.3g

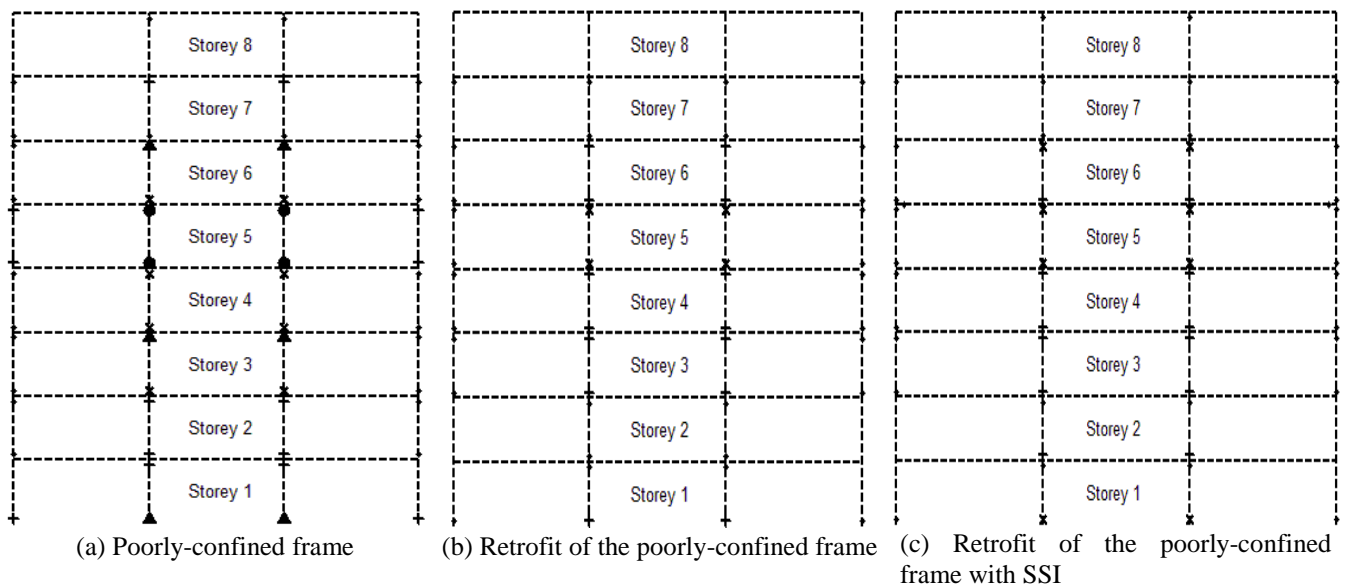


Fig. 13 Damage modes of 8-storey frames under seismic intensity 0.45g

FRP-confined retrofitted frame with fixed bases and 3) the FRP-confined retrofitted frame with SSI. Each case is analysed for three seismic intensities of 0.3g, 0.45g and 0.6g. Each intensity is represented by the above 14 selected scaled ground motions.

Under each earthquake excitation, hysteretic behaviours of nonlinear LINK elements are captured and then the damage imparted to the structure is quantified using a damage model. The damage model proposed by Cao *et al.* (2014) shown in Eq. (24) is used in this paper because the

Table 3 Damage levels

Legend	Damage index	Description
.	0 - 0.05	No or minor
+	0.05 - 0.25	Light
x	0.25 - 0.50	Moderate
▲	0.50 - 0.75	Severe
●	0.75 - 1.00	Collapse

damage index (DI) obtained from this model varies from 0 (no damage) to 1 (collapse) and increase with increasing force, deformation or number of cycles.

$$DI = \left[\frac{E_h}{E_h + E_{rec}} \right]^{\alpha(N-i)} \quad (24)$$

where, E_h is the cumulative hysteretic energy; E_{rec} is the cumulative recoverable energy; $N = \frac{E_{h,collapse}}{E_{h,ly}}$ is the

equivalent number of yielding cycles to collapse while $i = \frac{E_h}{E_{h,ly}}$ is the equivalent number of yielding cycles at the

current time of loading ($i \leq N$); $E_{h,collapse}$ and $E_{h,ly}$ are the hysteretic energy of one complete ultimate and yielding cycle, respectively; α is a modification factor and is proposed as 0.06 and the damage levels are shown in Table 3. The legends in the first column corresponding to their damage indices and damage descriptions in Table 3 are used to plot the damage distribution in frames.

For each seismic intensity represented by 14 ground motions, the corresponding 14 damage indices are obtained for a nonlinear LINK element. The damage index for that LINK is the average damage index of the above 14 damage indices. After the damage indices of all LINKs are obtained, the distribution of these damage indices in the frames are plotted as shown in Figs. 12-14. It is worth mentioning that

the damage levels presented in these Figs. are noted in the first column of Table 3. As can be seen, the most severe damage occurs at the storey 5 while the least damage occurs at the top storey. The damage in the two inner columns is more critical than the damage in the external columns of the same storey. The maximum damage indices in each storey are also determined and plotted in Figs. 15-17. Storey 1 is more damage than storey 2, which may be due to higher axial forces and moments on the columns of the first storey than columns of the second storey.

Figs. 12-17 show the damage states, expressed by damage indices, of the FRP retrofitted frame with and without SSI in comparison to the original poorly-confined frame without SSI experienced different seismic intensities. These Figs. exhibit the two following substantial aspects:

- The damage of the FRP retrofitted frame with and without SSI is much lower comparing to that of the original poorly-confined frame without SSI, making positive changes on the damage states of the FRP retrofitted frame. This reduction of damage results from the FRP wrap confinement effect.
- The damage of the FRP retrofitted frame with SSI increases comparing to the damage of that frame without SSI; thus, SSI demonstrates its detrimental effect. This detrimental effect generally increases with increasing of the seismic intensity; probably, because the SSI becomes more effective.

Specifically, for the seismic intensity of 0.3g and without SSI, the poorly-confined frame and its retrofit suffers moderate damage and light damage, respectively. When the SSI effect is considered, the damage of the retrofitted frame slightly increases. For the seismic intensity of 0.45g, the poorly-confined frame reaches the collapse state while the retrofitted frame sustains moderate damage. Due to the confinement effect of the FRP retrofit, the damage is significantly decreased from collapse to moderate; consequently, the damage state of the poorly-confined frame is brought down two damage levels. With

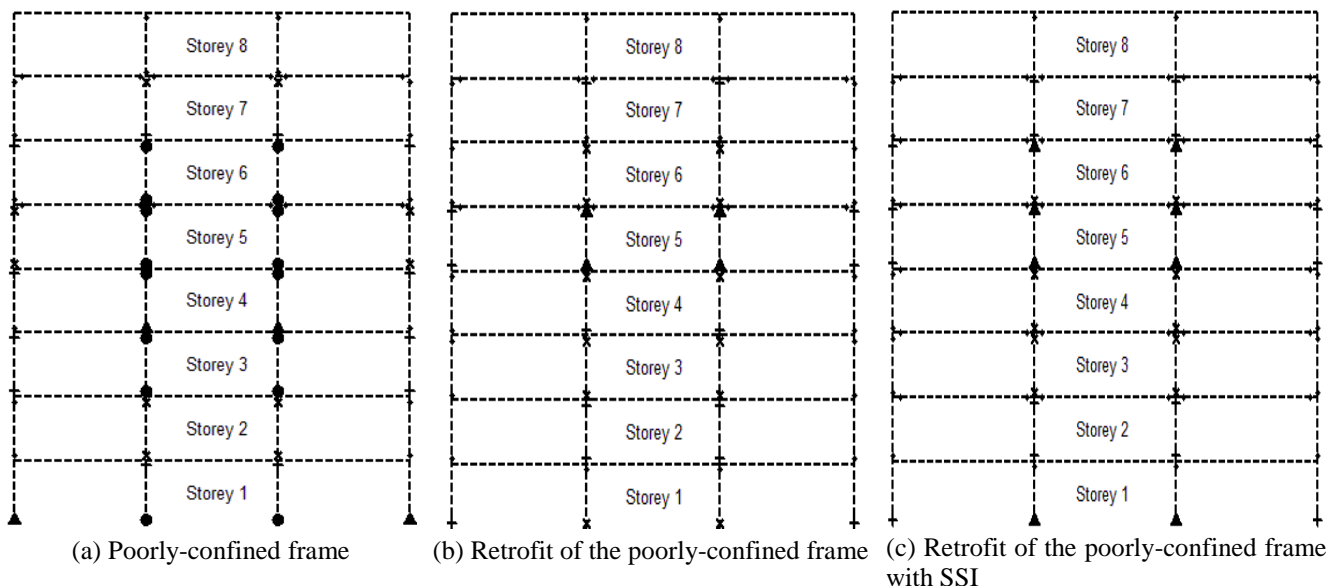


Fig. 14 Damage modes of 8-storey frames under seismic intensity 0.6g

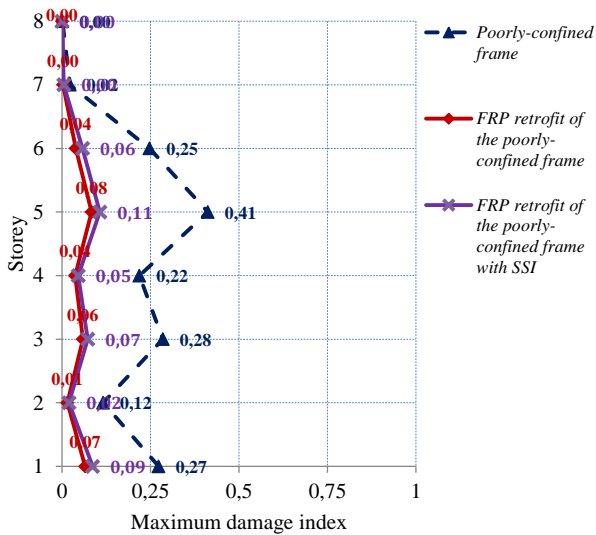


Fig. 15 Distribution of maximum damage indices of 8-storey frames under seismic intensity 0.3g

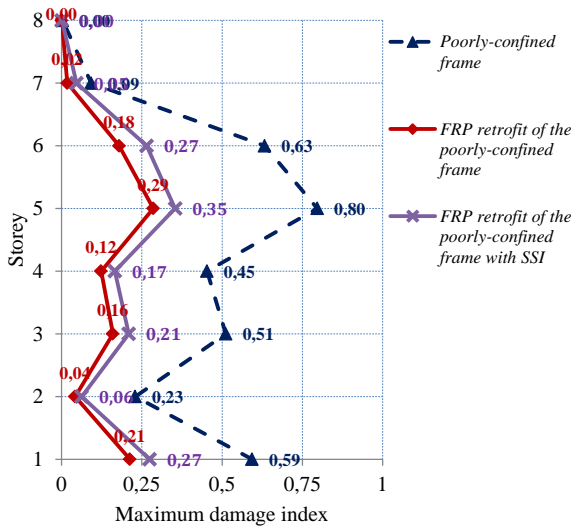


Fig. 16 Distribution of maximum damage indices of 8-storey frames under seismic intensity 0.45g

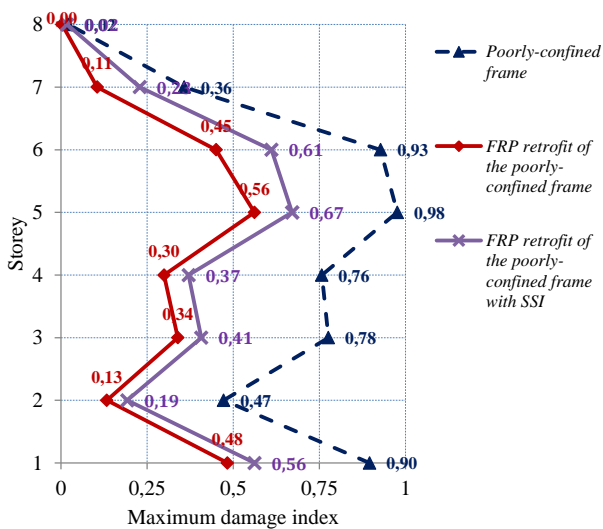


Fig. 17 Distribution of maximum damage indices of 8-storey frames under seismic intensity 0.60g

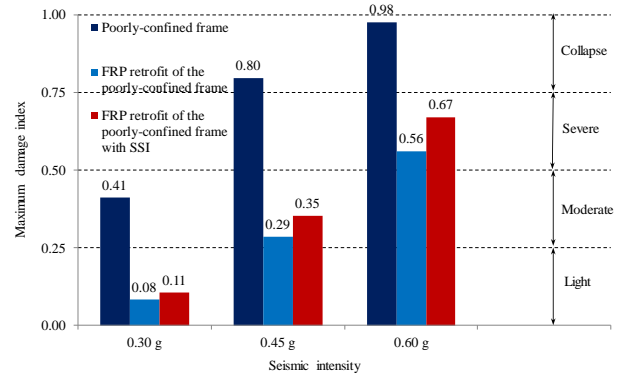


Fig. 18 Comparison of maximum damage indices

Table 4 Reduction of damage indices

Seismic intensity	$DI_{retrofitted} - DI_{original}$ (without SSI)	$DI_{retrofitted with SSI} - DI_{retrofitted without SSI}$
0.30 g	0.33	0.03
0.45 g	0.51	0.06
0.60 g	0.42	0.11

Table 5 Explanation example for the detrimental effect of SSI

Structure	First period (s)	Second period (s)	Third period (s)
Structure with fixed bases	1.5	1.3	1.0
Structure with SSI	1.73	1.50	1.15

the SSI effect, the damage of the retrofitted frame increases from 0.29 to 0.35. For the seismic intensity of 0.6g, the collapse of the poorly-confined frame reduces to the severe damage state of the retrofitted frame. When the SSI is considered, the damage index of the retrofitted frame increases by 0.11 from 0.56 to 0.67.

The damage indices of the FRP retrofitted frame is significantly reduced in comparison to the original one as shown in Fig. 18 and Table 4. If the poorly-confined frame is retrofitted by FRP confinement and is subjected to the seismic intensities of 0.30g, 0.45g and 0.60g, its damage index is reduced by 0.33, 0.51 and 0.42, respectively. This reduction of damage indices makes substantially positive changes on damage states of the poorly-confined RC frames and thus, demonstrates the effectiveness of FRP confinement retrofit.

Due to the SSI effect, the damage index of the FRP retrofitted frame increases by 0.03, 0.06 and 0.11 for seismic intensities of 0.30g, 0.45g and 0.60g, respectively. These increases of damage index are shown in Table 4 and Fig. 18. This detrimental effect contradicts the concept in current seismic design codes in which SSI is considered to be beneficial and the design base shear force is consequently reduced. The contradiction can be explained as follows. The current seismic code dealing with SSI employs the results of SDOF system. The response of elastic SDOF systems may inaccurately reflect the inelastic and nonlinear response of structures due to damage during earthquake excitations. Furthermore, though the first mode is important, contribution of higher modes is non-negligible

for multistorey buildings. Thus, evaluating the multistorey structures based solely on the first mode may lead to erroneous conclusions. SSI multi-storey structure system results in more damage because the SSI increases not only the fundamental period but also the higher mode periods. Consequently, higher modes become increasingly important in contribution to the response of structures. An example can be made for a structure with the first, second and third periods shown in Table 5. It is worth mentioning that these example periods are used for the purpose of explanation and clarification. If $\lambda=1.15$ due to SSI effect, the second period 1.3 s increases to 1.5 s which is equal to the first mode of the fixed base structure. Contribution of this second mode, together with the first mode 1.73 s, to the response of the structure becomes crucially important during an earthquake excitation. Increase in periods of higher modes, together with the elongated fundamental period, brings detrimental responses to structures.

5. Conclusions

Inelastic time history and damage analyses were conducted for the poorly-confined frame retrofitted by FRP wraps subjected to different seismic intensities with and without SSI. These analyses were also performed for the original frame for comparison. The results show that damage indices of the retrofitted frame are significantly reduced comparing to those of the original frame, positively changing the damage states and bringing down one or two damage levels for the retrofitted poorly-confined frame. Therefore, the FRP external confinement is an appropriate solution to retrofit RC structures poorly-confined due to transverse reinforcement deficiency. More importantly, the SSI effect is found to increase the potential damage of the FRP retrofitted frame; consequently, the effectiveness of the FRP retrofitting is reduced. This finding should be concerned for evaluating, strengthening or upgrading RC structures using FRP. In addition, the outcome of the current paper, together with the results from other researchers reported for RC structures, indicates that the conventionally beneficial concept of SSI, which has governed in structural and earthquake engineering for many decades, should be changed. More research is encouraged to fully address the issues of SSI effect on different FRP retrofitted structures.

Acknowledgements

This research is funded by Vietnam National Foundation for Science and Technology Development (NAFOSTED) under grant number 107.02-2017.18.

References

ACI (2008), Building Code Requirements for Structural Concrete (ACI 318M-08) and Commentary, 38800 Country Club Drive, Farmington Hills, American Concrete Institute, MI 48331, U.S.A.
 Adibi, M., Marefat, M.S., Arani, K.K. and Zare, H. (2017),

“External retrofit of beam-column joints in old fashioned RC structures”, *Earthq. Struct.*, **12**(2), 237-250.
 ASCE (2000), Prestandard and Commentary for the Seismic Rehabilitation of Buildings, Prepared for Federal Emergency Management Agency, FEMA Publication No. 356, Washington, D.C., Federal Emergency Management Agency.
 ASCE (2010), Minimum Design Loads for buildings and other structures, ASCE/SEI 7-10, American Society of Civil Engineers.
 Avilés, J. and Pérez-Rocha, L.E. (2003), “Soil-structure interaction in yielding systems”, *Earthq. Eng. Struct. Dyn.*, **32**(11), 1749-1771.
 Baji, H. (2017), “Calibration of the FRP resistance reduction factor for FRP-confined reinforced concrete building columns”, *J. Compos. Constr.*, **21**(3), 04016107.
 Baji, H., Ronagh, H.R. and Li, C.Q. (2016), “Probabilistic design models for ultimate strength and strain of FRP-confined concrete”, *J. Compos. Constr.*, **20**(6), 04016051.
 Balsamo, A., Colombo, A., Manfredi, G., Negro, P. and Prota, A. (2005), “Seismic behavior of a full-scale RC frame repaired using CFRP laminates”, *Eng. Struct.*, **27**, 769-780.
 Bielak, J. (1971), “Earthquake response of building-foundation systems,” Ph.D., California, Retrieved from <http://authors.library.caltech.edu/26407/1/7104.pdf> .
 Cao, V.V. and Ronagh, H.R. (2014), “Reducing the seismic damage of reinforced concrete frames using FRP confinement”, *Compos. Struct.*, **118**, 403-415.
 Cao, V.V., Ronagh, H.R., Ashraf, M. and Baji, H. (2014), “A new damage index for reinforced concrete structures”, *Earthq. Struct.*, **6**(6), 581-609.
 Chopra, A.K. and Gutierrez, J.A. (1974), “Earthquake response analysis of multistorey buildings including foundation interaction”, *Earthq. Eng. Struct. Dyn.*, **3**(1), 65-77.
 Computers and Structures Inc (2017), SAP2000 Version 19.2.0.
 De Luca, A., Nardone, F., Matta, F., Nanni, A., Lignola, G.P. and Prota, A. (2011), “Structural evaluation of full-scale FRP-confined reinforced concrete columns”, *J. Compos. Constr.*, **15**(1), 112-123.
 Di Ludovico, M., Manfredi, G., Mola, E., Negro, P. and Prota, A. (2008), “Seismic behavior of a full-scale RC structure retrofitted using GFRP laminates”, *J. Struct. Eng.*, **134**(5), 810-821.
 Di Ludovico, M., Prota, A., Manfredi, G. and Cosenza, E. (2008), “Seismic strengthening of an under-designed RC structure with FRP”, *Earthq. Eng. Struct. Dyn.*, **37**, 141-162.
 Dutta, S.C., Bhattacharya, K. and Roy, R. (2004), “Response of low-rise buildings under seismic ground excitation incorporating soil-structure interaction”, *Soil Dyn. Earthq. Eng.*, **24**(12), 893-914.
 Eslami, A. and Ronagh, H.R. (2013), “Effect of FRP wrapping in seismic performance of RC buildings with and without special detailing-A case study”, *Compos. Part B: Eng.*, **45**(1), 1265-1274.
 FEMA750 (2009), NEHRP Recommended Provisions for Seismic Regulations for New Buildings and Other Structures, Federal Emergency Management Agency.
 Flogeras, A.K. and Papagiannopoulos, G.A. (2017), “On the seismic response of steel buckling-restrained braced structures including soil-structure interaction”, *Earthq. Struct.*, **12**(4), 469-478.
 Garcia, R., Hajirasouliha, I. and Pilakoutas, K. (2010), “Seismic behaviour of deficient RC frames strengthened with CFRP composites”, *Eng. Struct.*, **32**, 3075 - 3085.
 Ghandil, M. and Behnamfar, F. (2017), “Ductility demands of MRF structures on soft soils considering soil-structure interaction”, *Soil Dyn. Earthq. Eng.*, **92**, 203-214.
 Güneş, E.M. and Azez, I. (2016), “Seismic upgrading of structures with different retrofitting methods”, *Earthq. Struct.*,

- 10(3), 589-611.
- Halabia, A.M. and Zafaran, M.M. (2014), "A new modal pushover analysis approach for soil-structure interaction", *Struct. Build.*, **168**(3), 210-234.
- Halabian, A.M. and Emami, A.R. (2014), "Effect of foundation flexibility on response of concrete frame structures under near-fault ground motions", *Struct. Build.*, **167**(2), 123-138.
- Harajli, M.H. and Rteil, A.A. (2004), "Effect of confinement using fiber-reinforced polymer or fiber-reinforced concrete on seismic performance of gravity load-designed columns", *ACI Struct. J.*, **101**(1), 47-56.
- Harajli, M.H., Hantouche, E. and Soudki, K. (2006), "Stress-strain model for fiber-reinforced polymer jacketed concrete columns", *ACI Struct. J.*, **103**(5), 672-682.
- Hassani, N., Baramia, M. and Ghodrati Amiri, G. (2018), "Effect of soil-structure interaction on inelastic displacement ratios of degrading structures", *Soil Dyn. Earthq. Eng.*, **104**, 75-87.
- Hawileh, R.A., Nawaz, W., Abdalla, J.A. and Saqan, E.I. (2015), "Effect of flexural CFRP sheets on shear resistance of reinforced concrete beams", *Compos. Struct.*, **122**(Supplement C), 468-476.
- ICBO (1994), Uniform Building Code, International Conference of Building Officials, Whittier, California.
- Jarernprasert, S. (2005), "An inelastic design approach for asymmetric structure-foundation systems", Ph.D., Carnegie Mellon University, Pittsburgh, PA.
- Jarernprasert, S., Bazan-Zurita, E. and Bielak, J. (2013), "Seismic soil-structure interaction response of inelastic structures", *Soil Dyn. Earthq. Eng.*, **47**, 132-143.
- Jennings, P.C. and Bielak, J. (1973), "Dynamics of building-soil interaction", *Bull. Seismol. Soc. Am.*, **63**(1), 9-48.
- Kakaletsis, D.J. (2016), "Comparative experimental assessment of seismic rehabilitation with CFRP strips and sheets on RC frames", *Earthq. Struct.*, **10**(3), 613-628.
- Kent, D.C. and Park, R. (1971), "Flexural members with confined concrete", *J. Struct. Div.*, **97**(7), 1969-1990.
- Kuntal, V.S., Chellapandian, M. and Prakash, S.S. (2017), "Efficient near surface mounted CFRP shear strengthening of high strength prestressed concrete beams-An experimental study", *Compos. Struct.*, **180**(Supplement C), 16-28.
- Lam, L. and Teng, J.G. (2003a), "Design-oriented stress-strain model for FRP-confined concrete", *Constr. Build. Mater.*, **17**, 471-489.
- Lam, L. and Teng, J.G. (2003b), "Design-oriented stress-strain model for FRP-confined concrete in rectangular columns", *J. Reinf. Plast. Compos.*, **22**(13), 1149-1186.
- Mason, H.B., Trombetta, N.W., Chen, Z., Bray, J.D., Hutchinson, T.C. and Kutter, B.L. (2013), "Seismic soil-foundation-structure interaction observed in geotechnical centrifuge experiments", *Soil Dyn. Earthq. Eng.*, **48**, 162-174.
- Mortezaei, A., Ronagh, H.R. and Kheyroddin, A. (2010), "Seismic evaluation of FRP strengthened RC buildings subjected to near-fault ground motions having fling step", *Compos. Struct.*, **92**, 1200-1211.
- Mylonakis, G. and Gazetas, G. (2000), "Seismic soil-structure interaction: beneficial or detrimental?", *J. Earthq. Eng.*, **4**(3), 277-301.
- Nakhaei, M. and Ali Ghannad, M. (2008), "The effect of soil-structure interaction on damage index of buildings", *Eng. Struct.*, **30**(6), 1491-1499.
- Park, R., Priestley, M.J.N. and Gill, W.D. (1982), "Ductility of square-confined concrete columns", *J. Struct. Div.*, **108**, 929-950.
- Paulay, T. and Priestley, M.J.N. (1992), *Seismic Design of Reinforced Concrete and Masonry Buildings*, John Wiley & Sons, New York.
- PEER. (2011), PEER ground motion database. http://peer.berkeley.edu/peer_ground_motion_database.
- Pellegrino, C. and Modena, C. (2010), "Analytical model for FRP confinement of concrete columns with and without internal steel reinforcement", *J. Compos. Constr.*, **14**(6), 693-705.
- Rahai, A. and Akbarpour, H. (2014a), "Experimental investigation on rectangular RC columns strengthened with CFRP composites under axial load and biaxial bending", *Compos. Struct.*, **108**(0), 538-546.
- Rahai, A. and Akbarpour, H. (2014b), "Experimental investigation on rectangular RC columns strengthened with CFRP composites under axial load and biaxial bending", *Compos. Struct.*, **108**(Supplement C), 538-546.
- Realfonzo, R. and Napoli, A. (2013), "Confining concrete members with FRP systems: Predictive vs design strain models", *Compos. Struct.*, **104**, 304-319.
- Reda, R.M., Sharaky, I.A., Ghanem, M., Seleem, M.H. and Sallam, H.E.M. (2016), "Flexural behavior of RC beams strengthened by NSM GFRP Bars having different end conditions", *Compos. Struct.*, **147**(Supplement C), 131-142.
- Rocca, S., Galati, N. and Nanni, A. (2009), "Interaction diagram methodology for design of FRP-confined reinforced concrete columns", *Constr. Build. Mater.*, **23**(4), 1508-1520.
- Ronagh, H.R. and Eslami, A. (2013), "On flexural retrofitting of RC buildings using GFRP/CFRP-A comparative study", *Compos. Part B*, **46**, 188-196.
- Sáez, E., Lopez-Caballero, F. and Modaresi-Farahmand-Razavi, A. (2011), "Effect of the inelastic dynamic soil-structure interaction on the seismic vulnerability assessment", *Struct. Saf.*, **33**(1), 51-63.
- Samaan, M., Mirmiran, A. and Shahawy, M. (1998), "Model of concrete confined by fiber composites", *J. Struct. Eng.*, **124**(9), 1025-1031.
- Shakib, H. and Fuladgar, A. (2004), "Dynamic soil-structure interaction effects on the seismic response of asymmetric buildings", *Soil Dyn. Earthq. Eng.*, **24**(5), 379-388.
- Sheikh, S.A. and Houry, S.S. (1993), "Confined concrete columns with stubs", *ACI Struct. J.*, **90**(4), 414-431.
- Sheikh, S.A. and Yau, G. (2002), "Seismic behavior of concrete columns confined with steel and fiber-reinforced polymers", *ACI Struct. J.*, **99**(1), 72-80.
- Smith, S.T., Kim, S.J. and Zhang, H. (2010), "Behavior and effectiveness of FRP wrap in the confinement of large concrete cylinders", *J. Compos. Constr.*, **14**(5), 573-582.
- Takeda, T., Sozen, M.A. and Nielsen, N.N. (1970), "Reinforced concrete response to simulated earthquakes", *J. Struct. Div.*, **96**, 2557-2573.
- Veletsos, A.S. and Meek, J.W. (1974), "Dynamic behaviour of building-foundation systems", *Earthq. Eng. Struct. Dyn.*, **3**(2), 121-138.
- Wang, L.M. and Wu, Y.F. (2008), "Effect of corner radius on the performance of CFRP-confined square concrete columns: Test", *Eng. Struct.*, **30**, 493-505.
- Wei, Y.Y. and Wu, Y.F. (2012), "Unified stress-strain model of concrete for FRP-confined columns", *Constr. Build. Mater.*, **26**, 381-392.
- Wu, G., Wu, Z.S. and Lü, Z.T. (2007), "Design-oriented stress-strain model for concrete prisms confined with FRP composites", *Constr. Build. Mater.*, **21**(5), 1107-1121.
- Youssef, M.N., Feng, M.Q. and Mosallam, A.S. (2007), "Stress-strain model for concrete confined by FRP composites", *Compos. Part B: Eng.*, **38**(5-6), 614-628.
- Zamani, N. and El Shamy, U. (2014), "A microscale approach for the seismic response of MDOF structures including soil-foundation-structure interaction", *J. Earthq. Eng.*, **18**(5), 785-815.